Electron energy loss and diffraction of backscattered electrons from silicon

2010 New J. Phys. 12 053001

(http://iopscience.iop.org/1367-2630/12/5/053001)

New Journal of Physics
The open-access journal for physics

Electron energy loss and diffraction of backscattered electrons from silicon

Aimo Winkelmann[1,3], **Koceila Aizel**[2] **and Maarten Vos**[2]

[1] Max-Planck-Institut für Mikrostrukturphysik, Weinberg 2, D-06120 Halle (Saale), Germany

[2] Research School of Physics and Engineering, Australian National University, Canberra, ACT, Australia

E-mail: winkelm@mpi-halle.mpg.de

New Journal of Physics **12** (2010) 053001 (18pp)
Received 15 February 2010
Published 5 May 2010
Online at http://www.njp.org/
doi:10.1088/1367-2630/12/5/053001

Abstract. Electrons backscattered from crystals can show Kikuchi patterns: variations in intensity for different outgoing directions due to diffraction by the lattice. Here, we measure these effects as a function of their energy loss for 30 keV electrons backscattered from silicon. The change in diffraction contrast with energy loss depends strongly on the scattering geometry. At steep incidence on the sample, diffraction contrast in the observed Kikuchi bands decreases rapidly with energy loss. For an energy loss larger than about 150 eV the contrast is more than 5 times less than the contrast due to electrons near zero energy loss. However, for grazing incidence angles, maximum Kikuchi band contrast is observed for electrons with an energy loss near 60 eV, where the contrast is more than 2.5× larger than near zero energy loss. In addition, in this grazing incidence geometry, the Kikuchi diffraction effects stay significant even for electrons that have lost hundreds of electron volts. For the maximum measured energy loss of 440 eV, the electrons still show a contrast that is 1.5 × larger than that of the electrons near zero energy loss. These geometry-dependent observations of Kikuchi band diffraction contrast are interpreted based on the elastic and inelastic scattering properties of electrons and dynamical diffraction simulations.

[3] Author to whom any correspondence should be addressed.

Contents

1. Introduction **2**
2. Experimental details **3**
3. Results **4**
3.1. Data analysis 4
3.2. Kikuchi band profiles and energy loss 7
4. Discussion **10**
5. Summary **16**
Acknowledgments **16**
References **17**

1. Introduction

Spectroscopic energy loss measurements of scattered electrons can provide analytical access to the physical properties of surfaces. This is due to a variety of possible interactions of the probe electrons with the target, such as plasmons, phonon or valence and inner shell excitations [1]–[4], as well as recoil losses (the transfer of kinetic energy from an electron to a nucleus in a large-angle electron deflection) [5, 6]. For high-resolution reflection energy loss spectroscopy (REELS) with primary electron energies in the order of few tens of keV [7]–[10], diffraction effects are important for crystalline and polycrystalline systems. These diffraction effects can result in reflection high-energy electron diffraction (RHEED) patterns [11] or Kikuchi patterns [12, 13].

Electron diffraction at these energies is increasingly used in practical material science applications in scanning electron microscopes (SEM) for local crystallographic characterization. A prominent method is electron backscatter diffraction (EBSD) [14]–[18]. Closely related to EBSD are the electron channeling patterns (ECP) [19]. The Kikuchi patterns that are measured in EBSD are fixed to the local crystallographic orientation and thus provide a reference for the grain orientation in polycrystalline materials, which is important e.g. for their mechanical properties.

EBSD patterns are recorded without dedicated energy resolution of the diffracted electrons. A conceptually very simple setup consisting of a phosphor screen and a sensitive CCD camera is used to collect backscattered electrons of all energies over an extended solid angle. For the large-angle scattering conditions used in EBSD, practically all elastically scattered electrons are scattered incoherently with respect to the incident beam. Hence, the Kikuchi patterns from incoherent sources observed in EBSD dominate over the coherent RHEED spot patterns, which can only be observed for small scattering angles.

Inelastic scattering leads to a redistribution of electrons over a large energy range, and it is currently not clear what energy range contributes to the diffraction contrast observed in an EBSD pattern. In order to quantitatively understand the pattern formation in EBSD and related techniques, we need more experimental information about the microscopic details of energy and momentum transfer in order to establish the degree to which coherence of the scattered electron waves can be sensed after multiple elastic and inelastic events. From a practical point of view, this question is closely linked to the thickness of the crystalline layer that is probed in an actual EBSD measurement, a quantity that is currently not well established.

To investigate this question in a systematic way, it is necessary to do angle-resolved REELS (or viewed differently: energy-resolved RHEED) at these energies [20]–[22]. A quantitative correlation between energy loss in REELS experiments and Kikuchi diffraction effects, however, is experimentally demanding since various spectrometer parameters have to be optimized at the same time: energy resolution of the order of <1 eV at energies of a few 10^4 eV, angular acceptance of the order of typical Bragg reflection angles and Kikuchi bandwidths (a few degrees), angular resolution of the order of the width of typical diffraction features (0.1 degree). It has been previously demonstrated how these requirements can be fulfilled by an electrostatic high-energy electron spectrometer [23]–[26].

Here, we present experimental results on the connection between energy loss and diffraction of backscattered electrons from silicon at primary beam energies of 30 keV, building on our recent initial investigations [26, 27]. Depending on the experimental geometry, we observe—maybe contrary to intuitive belief—that electrons that have created inelastic excitations can actually show more pronounced diffraction effects than those that are only elastically scattered. The experimental results can be explained using the general features of elastic and inelastic differential cross sections at keV energies and arguments from dynamical electron diffraction theory. We use dynamical electron diffraction simulations to support our analysis.

2. Experimental details

The experimental set up was developed for high-resolution electron momentum spectroscopy [23]. In the present study, the electrons emitted from gun B were detected for a constant scattering angle of 135.7° by a hemispherical electrostatic analyzer that has an energy resolution better than 0.5 eV at 25–40 keV primary beam energy (figures 1 and 2). The diameter of the electron beam is 0.25 mm.

The setup allows angle-resolved detection of electrons on a cone with half-opening angle $\theta_{\text{scat}} = 44.3°$, with azimuthal angles ϕ on that cone in the range of $\Delta\phi \approx \pm 5°$ (measured from the plane given by gun B and the central entrance of the electron energy analyzer, see figure 2). The angular sensitivity is provided by a position-sensitive detector consisting of channel plates and a resistive anode. The position-sensitive detector is calibrated for energy and ϕ as described in [23].

In the present experiments, we used primary electron energies of 30 keV and we detected electrons with losses of up to 440 eV. We used an Si(001) sample, which was treated by 2 keV Xe sputtering and subsequent annealing to more than 900 K by electron beam heating from the back of the sample holder.

The spectra measured show a distinct very intense peak at the low energy loss side. This is the elastic peak, and in most of the REELS literature it is assumed to be at zero energy loss. However, for the current kinematic conditions (30 keV e^- scattering over 135°), the kinetic energy transferred from an incident electron to an Si atom is close to 2 eV (recoil loss) [5, 6]. As all detected electrons have scattered elastically and thus experienced similar recoil losses, the whole spectrum is shifted by this amount. This small uniform shift does not affect any of the effects discussed in this paper, and for simplicity we shift the energy scale of the spectra such that the elastic peak is at zero energy loss. The relative contribution of the scattering processes with elastic energy loss to single atoms compared to coherent scattering by the whole crystal can be estimated from the Debye–Waller factor. For large-angle scattering, the Debye–Waller factor is extremely small, quantifying the reduction in coherent scattering from the crystal [28].

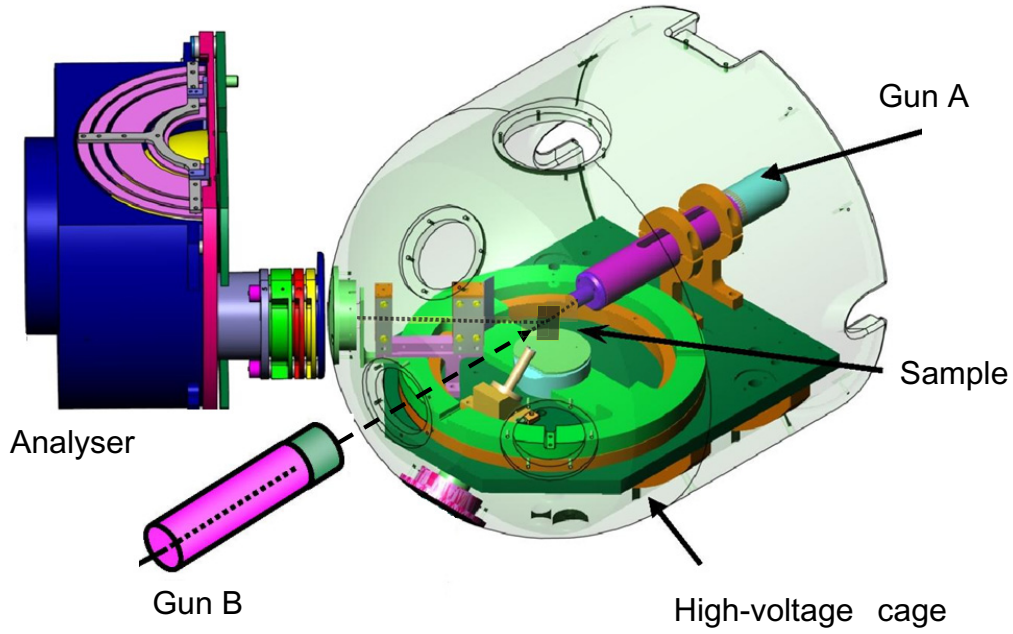

Figure 1. Experimental setup used in the present study. The electrostatic analyzer detects electrons scattered over a fixed angle from the direction of gun B (beam diameter 0.25 mm; gun A is not used in the present measurements). Rotation of the sample around the perpendicular axis changes the incidence direction and the outgoing direction with respect to the crystal correspondingly. The electrostatic analyzer has an energy resolution of 0.5 eV at 25–40 keV primary beam energy (for the schematic geometry defining the various angles, see figure 2).

An example of spectra obtained with this spectrometer is given in figure 3 for a measurement with the incoming beam aligned with the surface normal for two different angular ranges of the analyzer. The sharp elastic peak is followed by a series of plasmon peaks. Surface plasmon intensities are weak for such energies and geometry. The spectra of the different angular ranges of the spectrometer were normalized to equal intensity at the largest energy loss of this measurement (440 eV). Clearly the shape of the spectra is different, and the origin of this difference will be investigated in detail in this paper.

3. Results

3.1. Data analysis

We measure the number of backscattered electrons as a function of energy and azimuthal angle ϕ. The raw data for energy losses of up to 400 eV are shown in figure 4(a) for polycrystalline Mo and in figure 4(b) for Si(001). While the variations in detector efficiency along the energy-dispersive dimension of the position-sensitive detector are averaged out by scanning the analyzer bias voltage [23], we still have to correct the spectra for efficiency variations along the

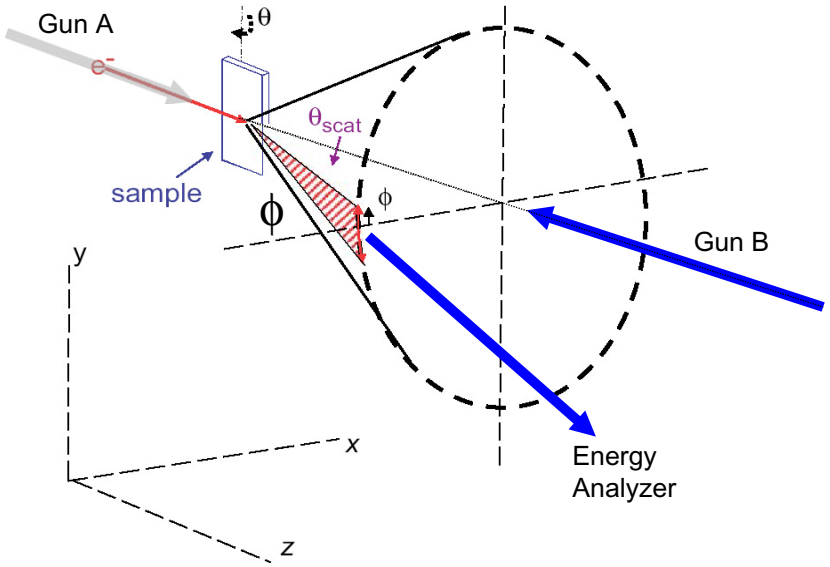

Figure 2. Experimental geometry. The electron energy analyzer accepts scattered electrons on a cone of azimuthal directions ϕ corresponding to a fixed scattering angle of $\theta_{\mathrm{scat}} = 44.3^\circ$ with respect to gun A and a scattering angle of 135.7° with respect to the incident direction of electron gun B used in the present experiment. The angular acceptance of the energy analyzer in ϕ is $\approx \pm 5^\circ$, with a resolution of $\Delta\phi \approx 0.1^\circ$ (compare with figure 1).

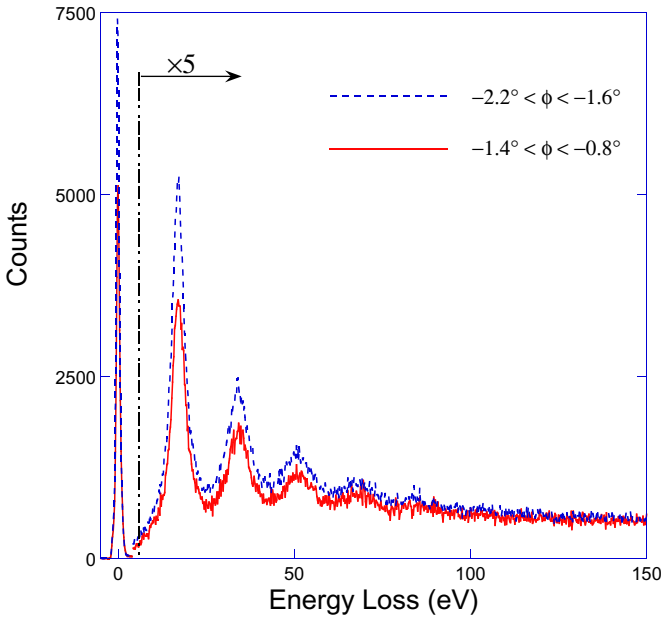

Figure 3. Spectra measured with the incoming beam aligned with the surface normal. Spectra obtained for two different ϕ ranges of the analyzer have different shapes.

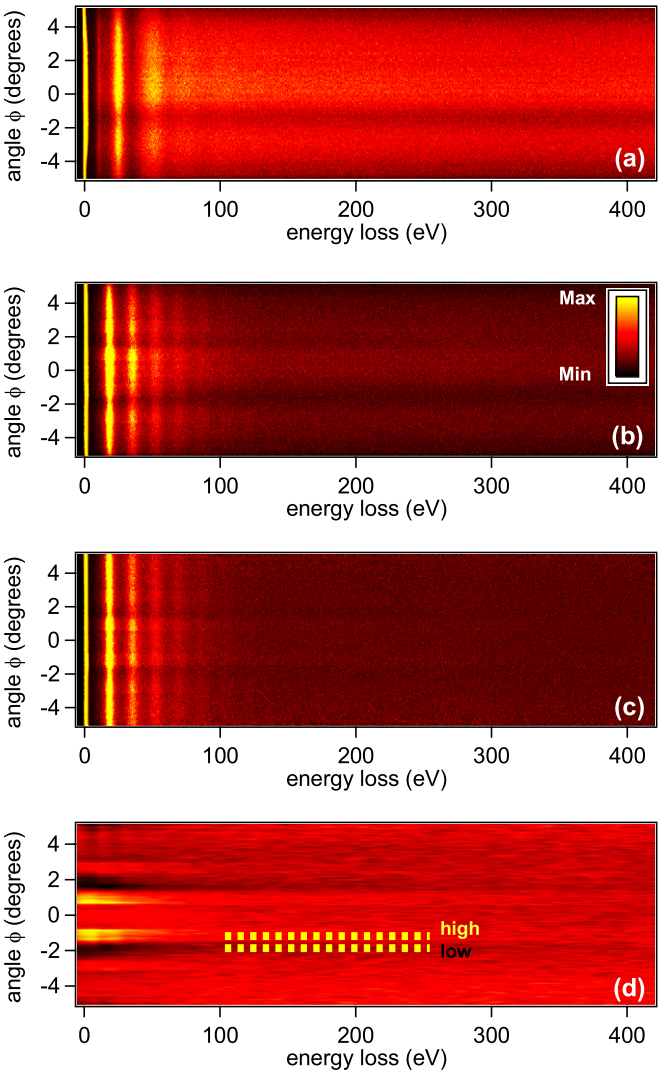

Figure 4. Data analysis procedure to obtain the diffraction signal. The energy loss is shown on the horizontal axis and the azimuthal angle ϕ on the vertical axis. (a) The number of detected electrons from polycrystalline Mo (sample holder) as a function of energy loss and azimuthal angle ϕ. (b) Si(001), normal incidence, scattering over 135.7°. (c) Si(001) data corrected for angular-dependent detector efficiency. (d) Pure diffraction signal from Si(001) data obtained after removing the electron energy loss structure by normalizing to the angular average at each energy loss.

angular-dispersive direction of the detection system, in order to identify the contribution that is due to diffraction. For the polycrystalline molybdenum sample holder, diffraction effects can be excluded (as many grains are sampled for our beam size) and the angular intensity distribution will only show the efficiency variation of the detector itself.

In the measured raw data for polycrystalline Mo in figure 4(a), we can clearly distinguish the elastic peak and the characteristic energy losses due to plasmon creation. The intensity variation on the vertical angular ϕ scale is due to the detection efficiency of the

position-sensitive detector (see also [26]). The *spectral* molybdenum energy loss structure from the intensities in figure 4(a) needs to be excluded for the correction of the *angular* variations in the data for silicon. Therefore, we self-normalize the Mo intensity at each measured energy loss by the respective ϕ-average along the vertical axis. We found that the resulting angular intensity variation can be considered as energy-independent, i.e. the angular sensitivity profile (excluding diffraction) is the same at each energy loss.

Using the angular sensitivity profile obtained from polycrystalline Mo, we can correct the raw Si data of figure 4(b). In this way, we obtain in figure 4(c) the angle-resolved EELS data for Si showing now the diffraction effects along the vertical axis. We can clearly distinguish an angular intensity distribution that is mirror-symmetric with a maximum around $\phi \approx 0^\circ$. The observed structure corresponds to the (220) Kikuchi band of Si. Besides the angular intensity variation, we see intensity variations along the horizontal axis. This is due to the energy loss spectrum of Si, which is dominated by the plasmon loss features at multiples of 17 eV (see also figure 3). In order to retain only the diffraction signal, we self-normalize the Si data by dividing the intensity at each energy by the ϕ-averaged intensity at that energy. The result is shown in figure 4(d), where we indicate regions of high (I_{high}) and low (I_{low}) intensity of the measured cross section of a Kikuchi band. Qualitatively, we already see that the diffraction effects are reduced for increasing energy losses in this measurement. We will demonstrate that this behavior changes if one rotates the sample and thus varies the incoming and outgoing angles of the measured electrons.

For quantification purposes, regions of high and low intensity (indicated in figure 4(d)) of a Kikuchi band profile are used for the experimental definition of the energy-loss-dependent contrast $C(E)$ as

$$C(E) = \frac{I_{\text{high}}(E) - I_{\text{low}}(E)}{I_{\text{high}}(E) + I_{\text{low}}(E)}. \tag{1}$$

3.2. Kikuchi band profiles and energy loss

We measured the energy-loss-dependent diffraction signal for a number of incidence angles of the primary beam. In figure 5, we show the diffraction signal for three different incidence angles: (a) 0°, (b) 45° and (c) 82° for energy losses up to 100 eV. Because of imperfect sample alignment, the symmetry line of the Kikuchi band moves slightly upwards on the ϕ-scale when going from 0° to 82° incidence angle. The incidence angles are adjusted by rotation of the sample, and correspondingly, the exit direction, and thereby the region of the detected Si(220) Kikuchi band, changes. This means that we see different Kikuchi profiles at each incidence angle, and the specific profile shape, and thus the absolute level of contrast, is different for each incidence–exit-angle combination. That is why we will discuss only the relative contrast variation in each separate geometry with respect to the contrast observed at zero energy loss.

In the measured data, we see that for 82° incidence (figure 5(c)), the elastically scattered electrons show less diffraction contrast than the inelastically scattered electrons with energy losses near 60 eV. This is in contrast to the result at normal incidence (figure 5(a)), where the electrons with no inelastic energy loss show the highest contrast. For the intermediate incidence angle of 45° (figure 5(b)), we can see that the diffraction contrast starts to extend to larger energy losses compared to normal incidence.

The characteristically different behaviors of the inelastically scattered electrons are seen clearly for selected energy-resolved diffraction profiles as shown in figure 6. Here, we compare

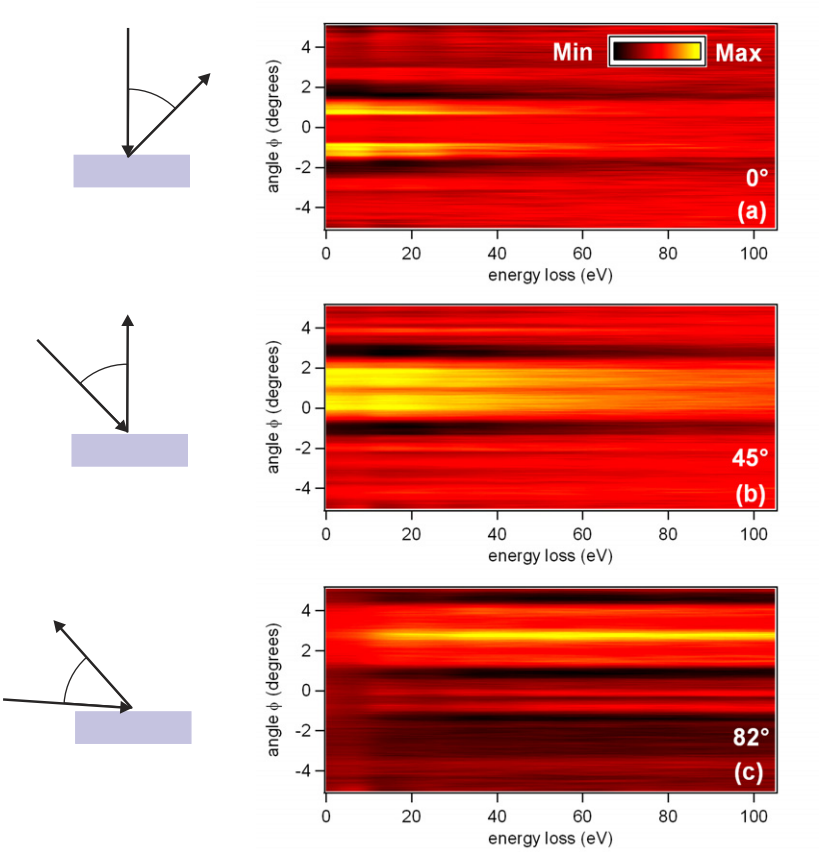

Figure 5. Energy-loss-dependent diffraction signal for three different incidence angles of (a) 0°, (b) 45° and (c) 82°. Note that for 82° incidence, the elastically scattered electrons show less diffraction contrast (note the blurred region near zero loss) than the inelastically scattered electrons with energy losses near 60 eV. Primary beam energy 30 keV. On the left, we show the corresponding experimental geometries with the sample, the incidence direction and the exit direction.

Kikuchi profiles for normal incidence with those for 82° incidence, for the elastic peak, electrons with one ($\Delta E = 17$ eV) and two plasmon losses ($\Delta E = 34$ eV), and electrons that have lost 400 eV. The intuitive expectation that the elastic peak electrons should show the most pronounced diffraction features is fulfilled at normal incidence, as is shown in the upper panel of figure 6, where the black solid line of the elastic peak shows the largest modulation. At 400 eV energy loss, the remaining diffraction variation is near the statistical limits of the current experiments. (This justifies the normalization procedure used for figure 3.) In surprising contrast to normal incidence, the 82° incidence measurement shows more modulation for the first and second plasmon losses than the elastic peak profile, and even at 400 eV energy loss the diffraction contrast is stronger than that of the elastic peak. Additionally, we clearly see that not only the modulation but also the sharpness of the features seen in the elastic Kikuchi profile is considerably reduced. The result for 82° incidence clearly seems to be counterintuitive in the usual connection of elastic scattering with diffraction. This seeming contradiction is resolved in the discussion below when taking into account that inelastic (energy loss) and elastic scattering (diffraction) can take place independently.

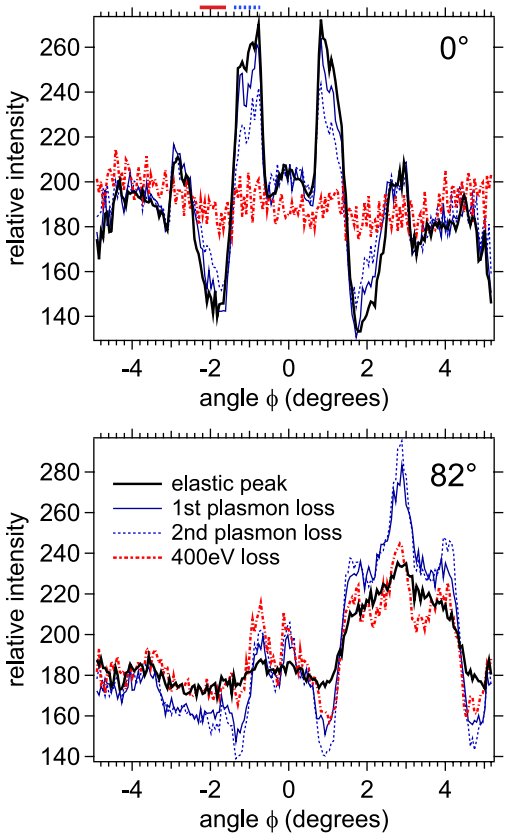

Figure 6. Kikuchi profiles for selected energy losses (normalized to the same mean intensity). At normal incidence (top panel), the highest contrast is seen for the elastically scattered electrons (heavy solid black). In contrast, at 82° incidence (bottom panel), the profiles for the first plasmon (solid blue) and second plasmon losses (dashed blue), and the electrons at 400 eV energy loss (dash-dotted red) clearly show more diffraction modulation (contrast) and sharpness than the elastically scattered electrons. Note that the different dependence of contrast on the energy loss at 0° and 82° is not caused by the different shapes of the Kikuchi band profiles, which are due to the different outgoing angles in experimental geometry of fixed incident and outgoing directions (see figure 2). The red and blue lines shown above the upper panel correspond to the angular integration ranges used in figure 3.

If we rotate the sample, then the outgoing directions measured by the analyzer correspond to different crystallographic directions. Hence, the shape and level of contrast of the observed Kikuchi bands change. As a consequence, we can only interpret the relative contrast changes for different sample rotations, that is, we calculate the normalized contrast at a given energy loss E by dividing the experimental contrast at that energy loss by the contrast at zero energy loss ($C(E)/C(0)$; see equation (1)). This normalized contrast for all measured incidence angles is shown in figure 7 for energy losses up to 440 eV. We can see a systematic change when going from normal incidence to more grazing incidence angles: a measurable diffraction contrast extends to larger and larger energy losses. As was already seen in the data presented above,

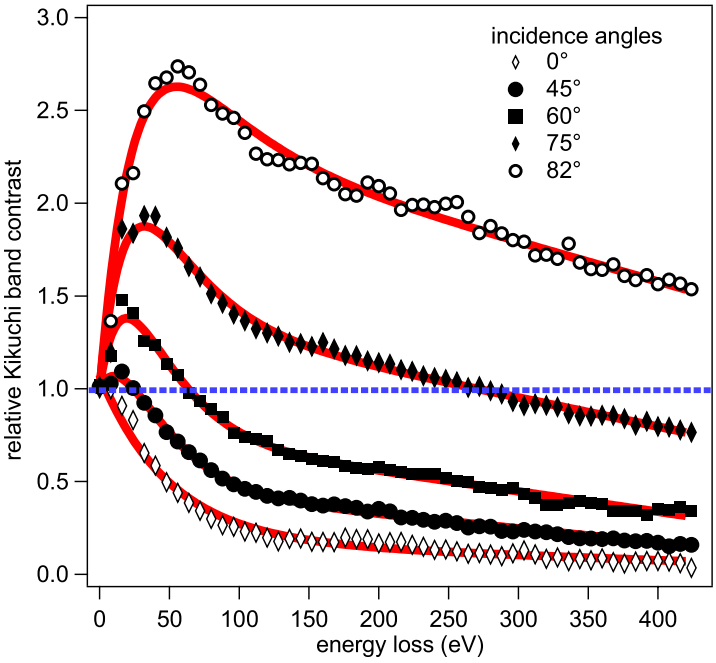

Figure 7. Summary of the incidence-angle-dependent measurements in this study. Observed contrast (relative to the elastic peak) as a function of energy loss for incidence angles from 0° to 82°. Solid red lines are guides to the eye. The dashed blue line indicates the contrast level of the elastic peak.

at 82° incidence the diffraction contrast of electrons with losses near 400 eV still show a higher contrast than the elastic ones (indicated by the dashed blue line in figure 7). We note qualitative similarities of the curve for 82° incidence with figure 4 in [29].

4. Discussion

In order to understand the results of the energy-resolved scattering experiments, we have to consider the different processes that determine the electron trajectories: inelastic and elastic scattering. The different properties of the differential (angle-dependent) elastic and inelastic cross section [30] can be used to gain insight into our results. We summarize the most important results:

- Inelastic scattering refers to energy loss of the keV electron due to the creation of internal electronic excitations in the target (e.g. plasmons in our experiment). At the electron energies we used in our experiment, *inelastic* scattering is *forward* scattering. Thus, inelastic scattering changes the energy, but has only a little effect on the direction of propagation ($\lesssim$ 10 mrad at 30 keV [1]).
- Elastic scattering refers to a change in direction of the trajectories due to the interaction with the potential of the atomic core. This interaction can cause large-angle deflection of the electron. For large-angle scattering of keV electrons, there is a small change in its energy due to momentum transfer to the scattering atom. This elastic energy transfer to a single Si atom is $\approx$2 eV for 135° scattering of a 30 keV electron. Applied to the system

of the 'incident electron' and the macroscopic 'backscattering crystal' as the scattering partners (instead of 'incident electron' and microscopic 'scattering atom'), this means that 2 eV are finally transferred to internal degrees of freedom (phonons) in the sample. In this macroscopic picture, the more accurate description of the backscattering events as sources for the Kikuchi pattern would be 'quasi-elastic' or 'thermal diffuse'. The fundamental microscopic interaction is, however, elastic scattering at the atomic cores with the concomitant recoil energy transfer.

Concerning the coherence of the electron waves in the various scattering processes, we note that large-angle scattering of keV electrons is mostly *incoherent* with respect to the incident electron wave as the available recoil energy for an atom is much larger than typical phonon energies of the crystal under observation [28]. For the detection of an electron in our backscattering experiment, at least one large-angle scattering event is a prerequisite. This is where the coherence to the incident beam will be lost. Small-angle scattering elastic scattering events occur as well, even much more frequently, as the cross section for forward elastic scattering is much larger. Forward elastic scattering involves much smaller momentum transfers (smaller recoil energy) compared to a backscattering event and thus the scattered waves can stay coherent with respect to each other to a larger degree. This is the basis for the observed diffraction effects of the incoming and outgoing electron waves.

We summarize these results into the following relations, which we assume to be valid under our experimental conditions:

interaction with target electrons	→	large energy loss and small change in direction
strong interaction with atomic cores	→	recoil loss and large change in direction
weak interaction with atomic cores	→	no energy loss and coherent forward scattering

In this scheme, inelastic scattering and large-angle elastic scattering lead effectively to a loss of the phase information of the scattered electron waves with respect to the electron wave before the scattering event. After the phase information is lost, the scattered electron waves can still interact with the crystal individually. The 'new' electron waves created by incoherent elastic backscattering all appear to emanate from atomic sites. As a consequence, their individual interference patterns with the crystal show the structures in the form of the Kikuchi patterns. In contrast, those 'new' electron waves that are created by inelastic plasmon scattering are more isotropically distributed over the unit cell, not just at the lattice atomic sites. Hence, their diffraction effects will tend to average out [31].

The Kikuchi patterns of a collection of incoherently backscattering point sources can be simulated using the dynamical theory of electron diffraction [32]. One important parameter here is the depth of the individual incoherent point source below the sample surface [31]. Without going into the details of dynamical electron diffraction theory at the moment, we can discuss the qualitative implications of the electron transport properties for the two scattering geometries of steep normal incidence and almost grazing incidence at 82° using figure 8. In the simplest case, an incoming electron changes its direction in only a single elastic backscattering event. This reverses the direction of the electron (by 135.7° in our experiment) and causes an elastic recoil energy loss of 2 eV if Si is the backscattering atom [6]. This process is shown in figure 8(a) (normal incidence) and figure 8(c) (82° incidence). After the incoherent backscattering, coherent elastic scattering (= diffraction) is taking place in the outgoing path, but this does not change the

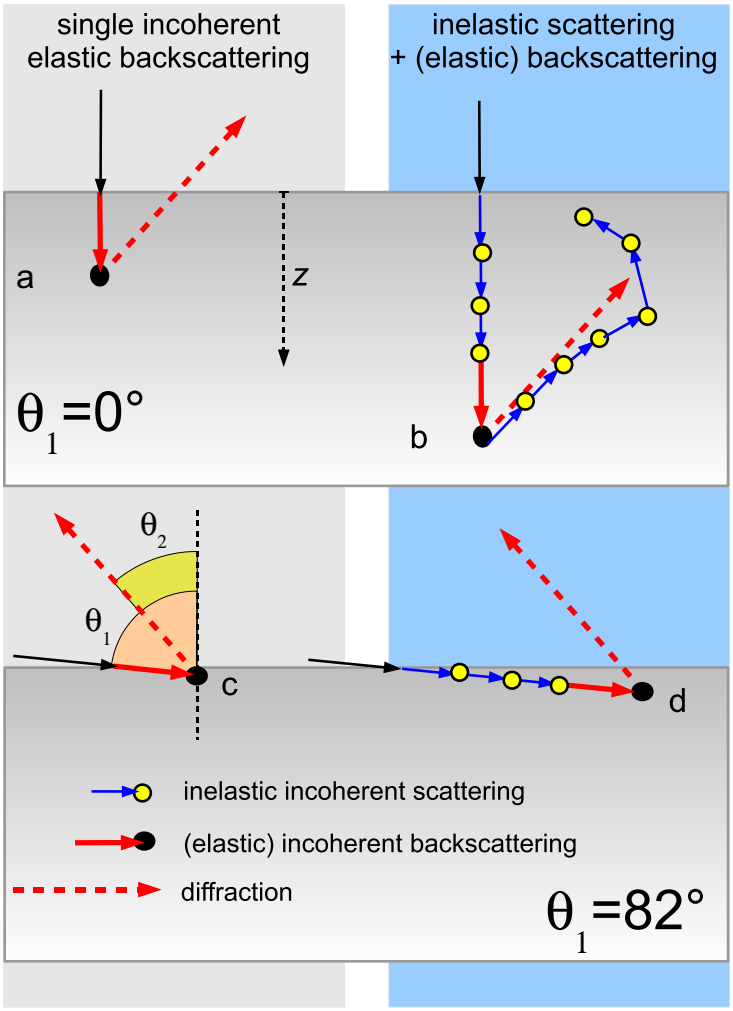

Figure 8. Comparison of the relevant scattering processes in geometries for incidence angles of 0° and 82°. At large incidence angles, single elastic backscattering (c) is taking place nearer to the surface compared to smaller incidence angles (a) and thus the diffraction features of the elastically scattered electrons are less pronounced due to the effectively reduced crystal thickness. At large incidence angles, inelastic scattering prior to a localized backscattering event can keep the electrons in the near surface region where they can be backscattered and subsequently diffracted without further inelastic scattering (d). At smaller incidence angles, inelastic scattering transports the electrons into deeper regions from which electrons cannot emerge without suppression of diffraction by additional inelastic scattering after the localized backscattering event (b).

energy of the scattered electron. We thus observe this electron in the elastic peak if no inelastic scattering occurs.

The electron will be detected at larger and larger energy loss as more inelastic scattering events occur. There is an important difference between inelastic scattering along the incoming direction and inelastic scattering along the outgoing direction. If phase information is lost due to inelastic scattering along the incoming direction, then this does not change the outcome of the

experiment, as phase information is lost anyway in the subsequent large-angle elastic scattering event. Loss of phase information due to inelastic scattering along the outgoing trajectory does affect the outcome of the experiments as these process is will reduce the contrast in the Kikuchi patterns.

In the two geometries, however, the ratios of the lengths of the incoming and outgoing trajectories are different. For normal incidence, the incoming trajectory is $\cos 0^\circ / \cos 44.3^\circ \approx 1.4$ times shorter than the outgoing trajectory, whereas in the tilted geometry it is $\cos(82^\circ - 44.3^\circ)/\cos(82^\circ) \approx 5.7$ times longer than the outgoing trajectory. This has severe implications in terms of the dynamical electron diffraction process. For the electrons observed in the elastic peak, the total path length (incoming plus outgoing) without inelastic scattering will be ultimately limited by the inelastic mean free path (≈ 40 nm for 30 keV e^- in Si [33, 34]). Due to the geometry at 82° incidence, the ingoing and outgoing parts of the shortest trajectories will be distributed roughly as 6:1. Considering the inelastic mean free path of 40 nm as characteristic, we obtain a distribution of 36 nm : 6 nm between the ingoing and outgoing path lengths. We know from dynamical diffraction theory that if the crystal thickness (the outgoing path length in our case) is below a quarter of the extinction distance [35] of the relevant reflection, the resulting Kikuchi diffraction features will be reduced in sharpness and contrast [31]. In simplified terms: if the crystal is too thin, then diffraction cannot be strong. For the (220) reflection in Si at 30 kV, the extinction distance is ≈46 nm (as calculated in the simulations below) and thus the length of the outgoing trajectories is well below a quarter of this value for the elastic peak of Si at the 82° measurement. This explains the observation of the reduced sharpness and lower contrast for the Kikuchi band profiles of the elastic peak in figure 6: these electrons at 82° originate from a depth that is too low for sharp diffraction patterns. In this respect, we are highly surface-sensitive when measuring the group of electrons shown in figure 8(c), although this comes at the price of less pronounced diffraction. Similar observations have been made using energy-filtered EBSD by Deal *et al* [29]. Trajectories with one inelastic event allowed have on average a length of two inelastic mean free paths. Thus, for the first and second plasmon features, the outgoing trajectories are also correspondingly longer, and the diffraction effects are better developed at 82° incidence.

In figures 8(c) and (d), we see how plasmon losses before backscattering can move the incoherent point source deeper into the crystal at grazing incidence without increasing the outgoing path length to a value where inelastic scattering (reduction in contrast) becomes important. This increased depth implies a larger crystal region above the source and results in the fuller development of dynamical diffraction effects. In this way, the sharper Kikuchi band profiles and higher contrast for the one and two plasmon loss features shown in figure 6 are caused.

With an increase in the number of plasmon losses, the backscattering depth reaches a value where inelastic losses in the outgoing path become important. This is more pronounced at 0° incidence, where the inelastic events are distributed more evenly over the outgoing and incoming trajectories, due to the geometric ratio of 1.4 : 1 as estimated above. Here, the effect of longer outgoing path length (sharper diffraction) is less important than the loss of electrons due to inelastic scattering events (less diffraction contrast), because already the electrons in the elastic peak are backscattered from deeper within the crystal (see below). In general, for energy losses larger than about 50 eV (corresponding to the creation of three plasmons or more in our experiments), the effect of more inelastic scattering along the outgoing trajectories is having a strong effect and that is why the contrast decreases for all geometries at larger energy losses (see figure 7).

In order to estimate the influence of the depth distribution of the incoherent Kikuchi pattern sources more quantitatively, we develop some simple model approximations, that will be the basis for dynamical diffraction simulations discussed afterwards. Based on the arguments in [36], we assume that elastic backscattering takes place in processes with V-type trajectories [37], which are dominated by a single large-angle scattering event, with additional scattering events on the incoming and outgoing paths. We will assume that the large-angle scattering events will create the incoherent sources, while the additional elastic scattering with the crystal in the outgoing path actually forms their Kikuchi patterns. We thus use the statistical Monte Carlo 'particle' picture to derive a simple average depth distribution of the incoherent large-angle scattering sources, which is then used as input for the subsequent quantum-mechanical treatment of diffraction in the 'wave' picture. This is a considerable simplification but leads to consistent results in the interpretation of our experiments, as we will show below.

The probability of N scattering events is assumed to be distributed according to a Poisson statistical process with mean free path λ and path length s:

$$W_N^{\mathrm{i/e}}(s) = (s/\lambda_{\mathrm{i/e}})^N \frac{\mathrm{e}^{-(s/\lambda_{\mathrm{i/e}})}}{N!}. \tag{2}$$

The simplest model case would be a depth distribution $\rho_{n_\mathrm{e}}^{n_\mathrm{i}}(z)$ given by single elastic incoherent backscattering $n_\mathrm{e} = 1$ distributed according to the process $W_1^\mathrm{e}(s)$ with elastic mean free path λ_e under the condition of $n_\mathrm{i} = 0$ inelastic events $W_0^\mathrm{i}(s)$ with inelastic mean free path λ_i. At the incidence angle θ_1 (see figure 8), the relative probability for backscattering at depth z is given by

$$\rho_1^0(z) = W_0^\mathrm{i}(z/\cos\theta_1) W_1^\mathrm{e}(z/\cos\theta_1). \tag{3}$$

In order to see the influence of inelastic forward scattering events on the depth distribution, we allow up to $n_\mathrm{i} = 2$ additional inelastic events on the incoming path:

$$\rho_1^{0,1,2}(z) = W_{0,1,2}^\mathrm{i}(z/\cos\theta_1) W_1^\mathrm{e}(z/\cos\theta_1). \tag{4}$$

We note here that the depth distribution $\rho_{n_\mathrm{e}}^{n_\mathrm{i}}(z)$ gives the number of backscattered electrons that starts from an incoherent point source at depth z below the surface. Inelastic scattering in the outgoing diffraction phase will additionally attenuate the intensity from the considered processes according to the outgoing path length by a factor of $W_0^\mathrm{i}(z/\cos\theta_2)$. This outgoing attenuation is treated by an imaginary part of the scattering potential in the dynamical diffraction simulation.

In figure 9, we show the normalized depth distributions for the two incidence angles of $\theta_1 = 0^\circ$ and $\theta_1 = 82^\circ$ calculated according to equation (4). For the elastic and inelastic mean free paths, we took the values of $\lambda_\mathrm{i} = 40\,\mathrm{nm}$ [33, 34] and $\lambda_\mathrm{e} = 24\,\mathrm{nm}$ [38] for Si at 30 keV. We can clearly see the increased surface sensitivity at shallow incidence compared to normal incidence. At 82° incidence, the single elastic scattering depth distributions for $n_\mathrm{i} = 0$ and $n_\mathrm{i} = 2$ can be approximated by an effective Poisson model with mean depth t_m:$\rho(z) \propto (z/t_\mathrm{m}) \times \exp(-z/t_\mathrm{m})$. Including the geometric depth enhancement factor of $1/\cos 37.7^\circ = 1.3$ due to the outgoing angle θ_2, we obtain $t_\mathrm{m} = 2.5\,\mathrm{nm}$ for $n_\mathrm{i} = 0$ and $t_\mathrm{m} = 7.6\,\mathrm{nm}$ for $n_\mathrm{i} = 2$.

Using these depth-dependent model distributions, we carried out dynamical simulations for silicon at 30 keV in order to show the correlation between the shape of the observed Kikuchi band profiles and the mean depth of backscattering in the measurements for 82° incidence. About 1000 reflections with minimum lattice spacing of 0.04 nm were included

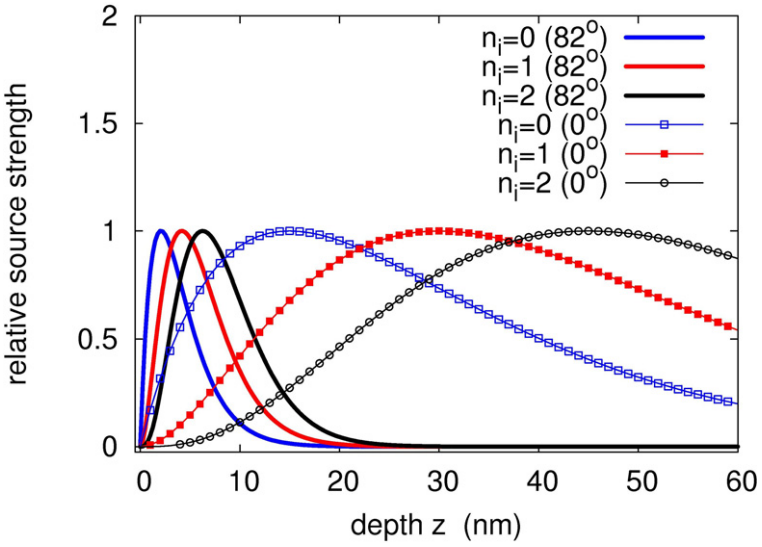

Figure 9. Thickness-dependent relative strength $\rho_{n_e}^{n_i}(z)$ of the Kikuchi pattern sources for normal incidence and for 82° incidence according to formula (4). The assumed number of inelastic scattering processes before backscattering is indicated by n_i.

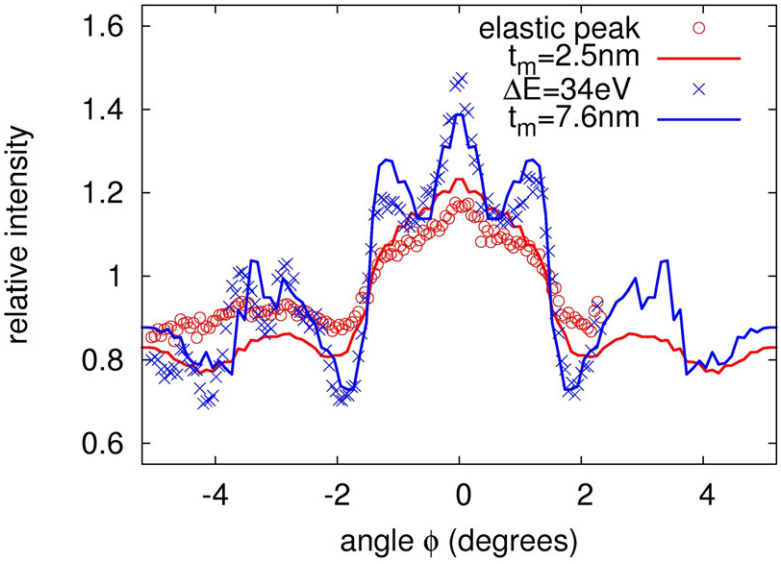

Figure 10. Simulated Kikuchi band profiles assuming a Poisson model for the backscattering depth distribution with mean depths of 7.6 nm (blue line) and 2.5 nm (red line) for 82° incidence. For comparison, we show the energy-dependent experimental data for the elastic peak (red circles) and the electrons at the second plasmon loss (blue crosses).

in the simulation [32, 39]. We used an effective Debye–Waller factor of 0.015 nm^2. We note that the only parameter changing was t_m for the two cases $n_i = 0$ and $n_i = 2$, respectively. As can be seen in figure 10, taking the $n_i = 2$, $t_m = 7.6$ nm distribution (solid blue line) leads to quite a reasonable agreement with the experimental measurements for the second plasmon loss

($\Delta E = 34$ eV). When the mean depth is reduced to $t_m = 2.5$ nm (solid red line), we see that the two peaks on the edge of the central Kikuchi band are disappearing. This is in agreement with the expectation that the elastic peak is sensitive to a thinner surface region than the electrons that have experienced plasmon losses and thus on average come from deeper regions. In agreement with the experimental data, the sharpness of the measured features is clearly reduced in the simulations for $t_m = 2.5$ nm. Due to our simple assumptions about the depth profile of the incoherent sources, we do not expect quantitative agreement of measurements and simulations. Nevertheless, the agreement with the experiments is good.

Already the simple model that we used above shows that via the measurement of *energy*-resolved diffraction profiles, we can gain access to *depth*-dependent transport of the elastically and inelastically scattered electrons. In this way, electron energy loss measurements can actually benefit from diffraction effects. We expect that, in a next step, the application of Monte Carlo simulations can give more realistic depth distributions of the incoherently backscattered electrons as a function of their energy loss. Ultimately, a quantitative simulation needs also to include diffraction of the incoming electron waves. The corresponding effects of the incoming beam have been neglected in the current analysis, since the numbers of backscattered electrons for different incidence angles have not been normalized with respect to each other. It should be possible, however, to account for these effects in future experiments.

5. Summary

Our investigations give quantitative insights into the details of EBSD pattern formation as a function of energy loss and should help us to analyze the possible limits of the current technique and the future possibilities of EBSD, potentially in energy-resolved modes [29]. Apart from the practical application in EBSD, our angle-resolved REELS measurements also provide reference data for quantitative theories of energy-resolved inelastic electron (back)scattering [40]–[44], which is one of the most general and difficult problems in electron diffraction theory.

As REELS measurements provide unique access to important properties of solid-state systems like the dielectric function [45, 46], a quantification of the influence of diffraction on these measurements is also necessary. Furthermore, electron momentum spectroscopy (EMS) of crystalline systems will benefit from a better understanding of diffraction effects [47, 48]. Since the Kikuchi pattern formation process in EBSD shares many common features with photoelectron diffraction, we can also expect that the presented measurements will be relevant for the interpretation of hard x-ray photoelectron diffraction (HXPD) experiments [49]. The ultimate combination of SEM technology with high-resolution electron energy loss spectroscopy and angle-resolved diffraction capability can be expected to provide improved possibilities of fundamental materials analysis. As a further application of high-resolution REELS experiments, we mention the proposal to achieve a *time* resolution of tens of femtoseconds via *energy*-resolved detection of diffracted intensities from chirped electron pulses that are initially excited by an ultrashort laser from a photocathode [50].

Acknowledgments

This work was made possible by a grant from the Australian Research Council. We thank Les Allen for stimulating discussions and the Atomic and Molecular Physics Laboratories at ANU for technical support.

References

[1] Egerton R F 2009 Electron energy-loss spectroscopy in the TEM *Rep. Progr. Phys.* **72** 016502
[2] Egerton R F 1996 *Electron Energy-Loss Spectroscopy in the Electron Microscope* 2nd edn (Berlin: Springer)
[3] Schattschneider P 1986 *Fundamentals of Inelastic Electron Scattering* (Berlin: Springer)
[4] Wang Z L 1996 *Reflection Electron Microscopy and Spectroscopy for Surface Analysis* (Cambridge: Cambridge University Press)
[5] Boersch H, Wolter R and Schoenebeck H 1967 Elastische Energieverluste kristallgestreuter Elektronen *Z. Phys.* A **199** 124–34
[6] Went M R and Vos M 2008 Rutherford backscattering using electrons as projectiles: underlying principles and possible applications *Nucl. Instrum. Methods Phys. Res.* B **266** 998–1011
[7] Powell C J and Swan J B 1959 Origin of the characteristic electron energy losses in aluminum *Phys. Rev.* **115** 869–75
[8] Schilling J 1976 Energieverlustmessungen von schnellen Elektronen an Oberflächen von Ga, In, Al und Si *Z. Phys.* B **25** 61–7
[9] Jablonski A 2005 Modeling of elastic and inelastic electron backscattering from surfaces *Prog. Surf. Sci.* **79** 3–27
[10] Werner W S M 2009 Electron transport for spectrum analysis and experiment design *J. Electron Spectrosc. Relat. Phenom.* at press, doi:10.1016/j.elspec.2009.09.004
[11] Ichimiya A and Cohen P I 2004 *Reflection High-Energy Electron Diffraction* (Cambridge: Cambridge University Press)
[12] Kikuchi S 1928 Diffraction of cathode rays by mica *Proc. Imper. Acad. Japan* **4** 354–6, http://www.journalarchive.jst.go.jp/jnlpdf.php?cdjournal=pjab1912&cdvol=4&noissue=7&startpage=354&lang=en&from=jnlabstract
[13] Alam M N, Blackman M and Pashley D W 1954 High-angle Kikuchi patterns *Proc. R. Soc.* A **221** 224–42, http://www.jstor.org/stable/100898
[14] Schwartz A J, Kumar M, Adams B L and Field D P (ed) 2009 *Electron Backscatter Diffraction in Materials Science* 2nd edn (Berlin: Springer)
[15] Wilkinson A J and Hirsch P B 1997 Electron diffraction based techniques in scanning electron microscopy of bulk materials *Micron* **28** 279–308
[16] Schwarzer R A 1997 Automated crystal lattice orientation mapping using a computer-controlled SEM *Micron* **28** 249–65
[17] Dingley D 2004 Progressive steps in the development of electron backscatter diffraction and orientation imaging microscopy *J. Microsc.* **213** 214–24
[18] Randle V 2008 Recent developments in electron backscatter diffraction *Adv. Imaging Electron Phys.* **151** 363–416
[19] Joy D C, Newbury D E and Davidson D L 1982 Electron channeling patterns in the scanning electron microscope *J. Appl. Phys.* **53** R81–122
[20] Krivanek O L, Tanishiro Y, Takayanagi K and Yagi K 1983 Electron energy loss spectroscopy in glancing reflection from bulk crystals *Ultramicroscopy* **11** 215–22
[21] Horio Y, Hashimoto Y and Ichimiya A 1996 A new type of RHEED apparatus equipped with an energy filter *Appl. Surf. Sci.* **100–101** 292–6
[22] Nakahara H, Hishida T and Ichimiya A 2003 Inelastic electron analysis in reflection high-energy electron diffraction condition *Appl. Surf. Sci.* **212–213** 157–61
[23] Vos M, Cornish G P and Weigold E 2000 High-energy (e, 2e) spectrometer for the study of the spectral momentum density of materials *Rev. Sci. Instrum.* **71** 3831–40
[24] Vos M 2001 Observing atom motion by electron-atom compton scattering *Phys. Rev.* A **65** 012703
[25] Vos M and Went M R 2008 Splitting the plasmon peak in high-energy reflection electron energy loss experiments *J. Electron Spectrosc. Relat. Phenom.* **162** 1–7

[26] Went M, Winkelmann A and Vos M 2009 Quantitative measurements of backscattered electron diffraction patterns using an electrostatic analyzer *Ultramicroscopy* **109** 1211
[27] Vos M, Aizel K and Winkelmann A 2010 Experimental observation of the strong influence of crystal orientation on electron Rutherford backscattering spectra *Surf. Sci.* at press, doi:10.1016/j.susc.2010.02.016
[28] Lipkin H J 1973 *Quantum Mechanics: New Approaches to Selected Topics* (Amsterdam: North-Holland)
[29] Deal A, Hooghan T and Eades A 2008 Energy-filtered electron backscatter diffraction *Ultramicroscopy* **108** 116–25
[30] Werner W S M 2001 Electron transport in solids for quantitative surface analysis *Surf. Int. Anal.* **31** 141–76
[31] Winkelmann A 2009 Principles of depth-resolved Kikuchi pattern simulation for electron backscatter diffraction *J. Microsc.* at press
[32] Winkelmann A 2009 Dynamical simulation of electron backscatter diffraction patterns *Electron Backscatter Diffraction in Materials Science* ed A J Schwartz, M Kumar, B L Adams and D P Field (Berlin: Springer) chapter 2, http://www.springer.com/cda/content/document/cda_downloaddocument/9780387881355-c2.pdf?SGWID=0-0-45-749108-p173906909
[33] Tanuma S, Powell C J and Penn D R 1993 Calculations of electron inelastic mean free paths. V. Data for 14 organic compounds over the 50–2000 eV range *Surf. Interface Anal.* **21** 165
[34] Powell C J and Jablonski A 1999 Evaluation of calculated and measured electron inelastic mean free paths near solid surfaces *J. Phys. Chem. Refer. Data* **28** 197–62
[35] De Graef M 2003 *Introduction to Conventional Transmission Electron Microscopy* (Cambridge: Cambridge University Press)
[36] Werner W S M 2005 Trajectory reversal approach for electron backscattering from solid surfaces *Phys. Rev.* B **71** 115415
[37] Yubero F, Pauly N, Dubus A and Tougaard S 2008 Test of validity of the V-type approach for electron trajectories in reflection electron energy loss spectroscopy *Phys. Rev.* B **77** 245405
[38] Browning R, Li T Z, Chui B, Jun Ye, Pease R F W, Czyżewski Z and Joy D C 1994 Empirical forms for the electron/atom elastic scattering cross sections from 0.1 to 30 keV *J. Appl. Phys.* **76** 2016–22
[39] Winkelmann A, Trager-Cowan C, Sweeney F, Day A P and Parbrook P 2007 Many-beam dynamical simulation of electron backscatter diffraction patterns *Ultramicroscopy* **107** 414–21
[40] Dudarev S L, Peng L M and Whelan M J 1993 Correlations in space and time and dynamical diffraction of high-energy electrons by crystals *Phys. Rev.* B **48** 13408
[41] Dudarev S L, Rez P and Whelan M J 1995 Theory of electron backscattering from crystals *Phys. Rev.* B **51** 3397
[42] Schattschneider P, Nelhiebel M, Souchay M and Jouffrey B 2000 The physical significance of the mixed dynamic form factor *Micron* **31** 333–45
[43] Schattschneider P, Jouffrey B and Nelhiebel M 1996 Dynamical diffraction in electron-energy-loss spectrometry: the independent bloch wave model *Phys. Rev.* B **54** 3861–8
[44] Schattschneider P and Jouffrey B 2003 Channeling, localization and the density matrix in inelastic electron scattering *Ultramicroscopy* **96** 453–62
[45] Went M R, Vos M and Werner W S M 2008 Extracting the Ag surface and volume loss functions from reflection electron energy loss spectra *Surf. Sci.* **602** 2069–77
[46] Werner W S M, Went M R, Vos M, Glantschnig K and Ambrosch-Draxl C 2008 Measurement and density functional calculations of optical constants of Ag and Au from infrared to vacuum ultraviolet wavelengths *Phys. Rev.* B **77** 161404
[47] Fang Z, Matthews R S, Utteridge S, Vos M, Canney S A, Guo X, McCarthy I E and Weigold E 1998 Electron-momentum spectroscopy of crystal silicon *Phys. Rev.* B **57** 12882–9
[48] Vos M, Kheifets A S, Bowles C, Chen C, Weigold E and Aryasetiawan F 2004 Electronic structure of copper studied by electron momentum spectroscopy *Phys. Rev.* B **70** 205111
[49] Winkelmann A, Fadley C S and Garcia de Abajo F J 2008 High-energy photoelectron diffraction: model calculations and future possibilities *New. J. Phys.* **10** 113002
[50] Baum P and Zewail A 2008 Femtosecond diffraction with chirped electron pulses *Chem. Phys. Lett.* **462** 14–7